Controllable Pt/ZnO Porous Nanocages with Improved Photocatalytic Activity

Haibo Zeng,* Peisheng Liu, Weiping Cai,* Shikuan Yang, and Xiaoxia Xu

Key Laboratory of Materials Physics, Anhui Key Laboratory of Nanomaterials and Nanotechnology, Institute of Solid State Physics, Chinese Academy of Sciences, Hefei 230031, P. R. China

Received: August 15, 2008; Revised Manuscript Received: October 11, 2008

Composite Pt/ZnO porous nanocages with ultrathin porous ZnO shell layers and ultrafine embedded Pt nanoparticles were facilely fabricated by ultrasonic irradiation-assisted two-step etching of Zn/ZnO core/shell nanoparticle colloids. The Pt cluster size can be well adjusted by the applied ultrasonic power. These Pt/ZnO nanocages exhibit excellent photocatalytic performance and can be further improved by the control of the embedded noble metal nanoparticles, which can be attributed to the abundant nanoscale Schottky contacts in the Pt−ZnO metal−semiconductor interfaces as well as to the large specific surface area due to the unique porous structure. The selective etching route used here could be of considerable universality for fabrication of a series of noble metal/oxide porous nanostructures as photocatalysts, such as the (Au, Ag, Pt, Pd)/(ZnO, TiO_2) system.

Introduction

Among semiconductor photocatalysts, besides the most extensively studied TiO_2, ZnO with a similar band gap (3.2 eV) has attracted much attention due to its high photosensitivity and stability.[1−3] Even ZnO has been shown to be more efficient in the photodegradation of some organic compounds. For instance, Sakthivel et al. compared the efficiency of TiO_2, ZnO, SnO_2, ZrO_2, α-Fe_2O_3, WO_3, and CdS, in the photodegradation of an azo dye (acid brown 14) aqueous solution using sunlight as the energy source, in which ZnO emerged as the most active photocatalyst.[4] Up to now, a major limitation of achieving high photocatalytic efficiency in semiconductor nanostructures has been the quick recombination of charge carriers.[5] Besides doping and forming solid solution semiconductors,[6] one probable resolving route is to develop composite nanostructures including semiconductor−semiconductor or semiconductor−metal types. Electrochemical[7] and photochemical[8] experiments have shown that the noble metal nanoparticles exhibit unusual redox activity by readily accepting electrons from a suitable donor. If such metal particles come in contact with a charged semiconductor nanostructure, they can equilibrate and undergo Fermi-level equilibration. Such electron transfer would greatly enhance the separation of photogenerated electrons and holes and hence improve the photocatalytic efficiency, as demonstrated in ZnO−Au nanoparticles,[9,10] Ag@TiO_2 core−shell composite clusters,[11] Ag/ZnO nanoparticles,[12] and mesoporous Au/TiO_2 nanocomposites.[13] Another improving approach for photocatalysis is to further increase the specific surface area of photocatalysts. From this aspect, photocatalysts with various morphologies and enhanced photocatalytic activity have been explored, such as ZnO nanoplatelets,[14] ZnO nanotetrapods,[15] and recently reported ZnO multisheets.[16] Compared with these nanoobjects with a solid interior, hollow structures have much larger specific surface area. Recently, Wang fabricated ZnO−SnO_2 microsized hollow spheres,[17] showing higher photocatalytic activity than solid nanorods.

In terms of the integration of the above two possible improving routes, the nanoscale hollow shells with semiconductor matrix and incorporated noble metal could have high photocatalytic activity. Recently, we have achieved the construction of pure ZnO and noble metal/ZnO hollow nanoparticles by one-step etching, and the latter exhibited improved photocatalysis efficiency and photostability in the photodegradation of methyl orange under ultraviolet light irradiation.[18] Along this idea, the refined structural adjustments on the semiconductor matrix and incorporated noble metal could result in the further improvement of their photocatalysis performance. Here, we report a facile but effective approach to fabricate Pt/ZnO porous nanocages and to control both the ZnO matrixes and the embedded Pt clusters through ultrasonic irradiation-assisted two-step etching. The shell matrixes were subtly etched into a porous state, and the incorporated Pt particle's average diameter was further reduced to about 1 nm, which surely induces the improvement of photocatalytic efficiency. The route developed here should be of considerable universality for a series of metal/oxide photocatalysts with fine controllability on matrixes and incorporators.

Experiments

The primal Zn/ZnO core/shell nanoparticle colloids were synthesized by laser ablation in liquid (LAL) as in our previous reports.[19] Briefly, a zinc plate (99.99%), immersed in 0.05 M sodium dodecyl sulfate aqueous solution, was ablated (irradiated) by the Nd:YAG laser (1064 nm, 10 Hz) with a 2 mm focusing spot for 30 min. The Pt/ZnO porous nanocages were fabricated by the two-step weak acid etching process of the Zn/ZnO nanoparticle colloids, accompanied by the durative ultrasonic irradiation in a JL360 commercial ultrasonic cleaner. First, chloroplatinic acid aqueous solution (H_2PtCl_6, 2 mM, 10 mL) was added into 50 mL of a primal colloid solution, droplet by droplet in 30 min with ultrasonic irradiation. Then, tartaric acid aqueous solution ($C_4H_6O_6$, 5 mM, 10 mL) was added in another 30 min with ultrasonic irradiation. Finally, additive ultrasonic irradiation was perserved for one hour. After etching, the colloidal solutions were centrifuged at 14 000 rpm and then ultrasonically redispersed in ethanol for more than five cycles

* Corresponding authors. E-mail: hbzeng@issp.ac.cn (H.Z.); wpcai@issp.ac.cn (W.C.).

10.1021/jp807309s CCC: $40.75
Published on Web 11/14/2008

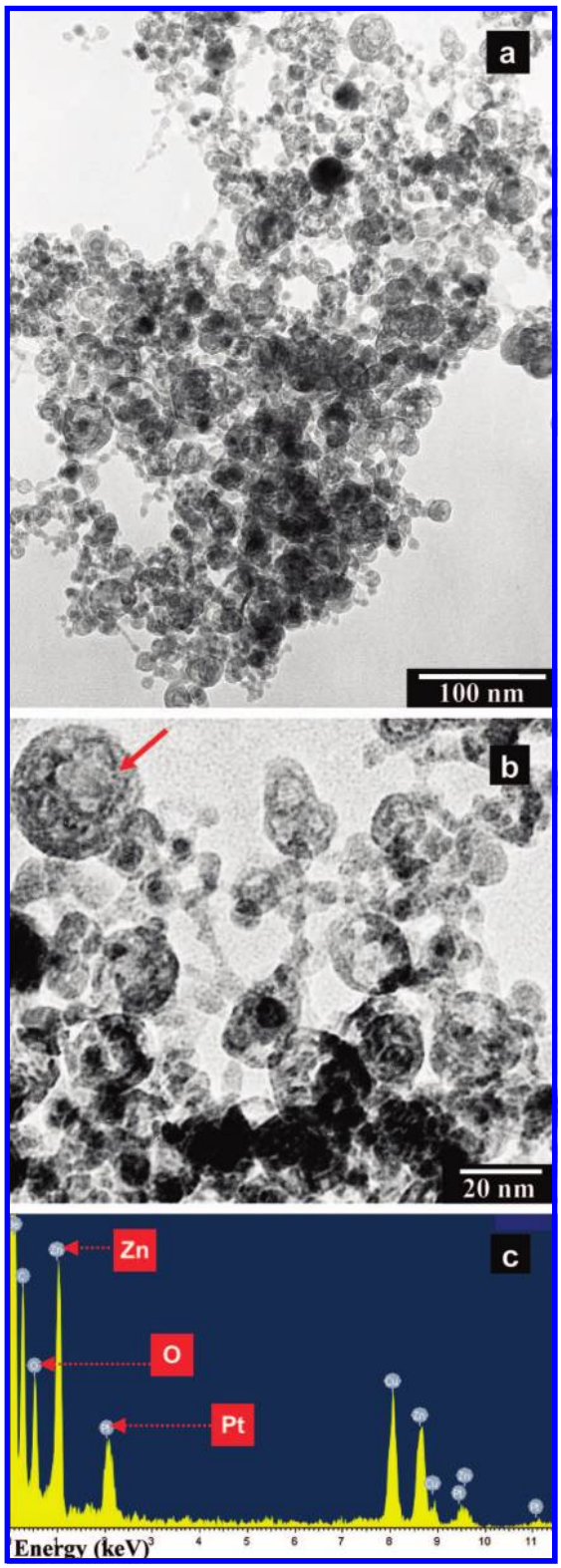

Figure 1. Low-magnification (a) and high-magnification (b) TEM images and EDX spectrum (c) of the Pt/ZnO porous nanocages obtained by ultrasonic irradiation assisted two-step etching.

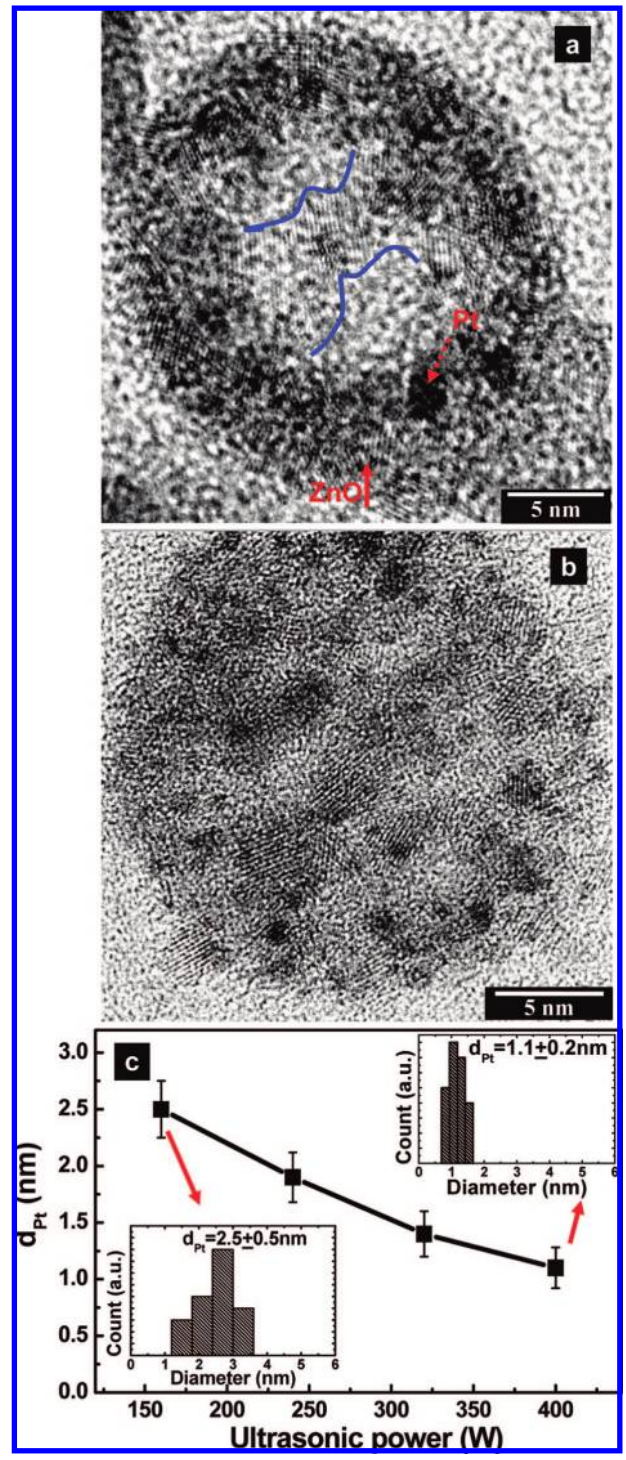

Figure 2. Typical HRTEM images of Pt/ZnO porous nanocages with corresponding applied ultrasonic power of 240 W (a) and 400 W (b), and the Pt particle diameter dependence (b) on the ultrasonic irradiation power.

to remove the surfactants, and finally draft-dried in an oven at 40 °C for 24 h.

The obtained powder samples were characterized by powder X-ray diffraction (XRD, Philips X'Pert with Cu Kα line of 0.15419 nm), transmission electron microscopy (TEM, JEM-200CX; HRTEM, JEOL-2010), and energy dispersive X-ray spectrum (EDX). The average diameter of the Pt nanoparticle was obtained by statistic value from more than 10 HRTEM images of nanocages. The optical absorption spectra were recorded by a Cary 5E UV−vis−IR spectrometer for the obtained colloidal solutions. The photocatalytic performance was evaluated by monitoring the optical absorption peak of methyl orange at 465 nm. Amounts of 10 mg of different catalyst powders were added into 10^{-5} M (20 mL) methyl orange aqueous solution and vigorously stirred for 30 min, and then the mixed solution was irradiated by an ultraviolet lamp with power of 125 W and center wavelength of 365 nm. Solutions

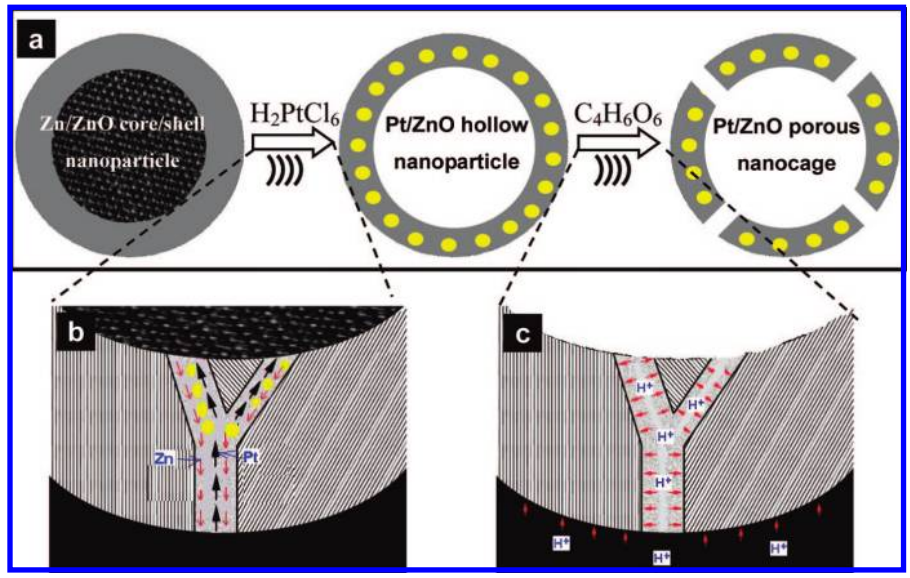

Figure 3. Illustration of the formation mechanism of Pt/ZnO nanocages: (a) total process description, (b) H_2PtCl_6 etching-induced diffusion−redox−deposition process, (c) $C_4H_6O_6$ etching-induced nanoshell opening.

of about 1 mL were taken out after different irradiation time for optical absorption measurements.

Results and Discussion

Figure 1 presents the typical characterizations of the products by the ultrasonic irradiation assisted two-step etching. The low-magnification image in Figure 1a demonstrates that the product is hollow nanoparticles with a porous surface, which is relatively pure in morphology and has a large yield. According to the statistics, the particle average diameter and shell thickness are about 20 and 3 nm, which is close to that of the primal nanoparticles before etching. More clearly, the high-magnification image in Figure 1b shows that the inners of these spherical particles have become hollow after etching of Zn/ZnO nanoparticle, but their shells have been obviously porous, typically demonstrated in the particle marked with the arrow. The EDX spectrum Figure 1c clearly demonstrates that the porous nanocages are composed of ZnO and Pt, but no separated Pt nanoparticles are found from the TEM observation in Figure 1a and b, which indicates that the Pt could have been incorporated into the ZnO porous shells during the etching process, forming the Pt/ZnO porous nanocages.

Further, the microstructure of the Pt/ZnO porous nanocage was revealed by the HRTEM image in Figure 2a and b. On one hand, the ZnO shell frames are found to be well crystalline according to their clear lattice fringes, but obviously porous. Typically in Figure 2a, ZnO crystals in the center of the particle are observed as a strap region to join the opposite shell walls, but two blanks exist in its two-side regions as the curves marked, forming the surface pores. Such information well demonstrates the transformation of a particle structure from solid sphere to porous cage. With the power of ultrasonic irradiation increasing up to 400 W, more surface pores can be seen in Figure 2b. On the other hand, the embedded Pt clusters (the dashed arrow) with high contrast due to their higher electron density than ZnO matrix (the solid arrow) can be easily seen in a large quantity in Figure 2a and b. Correspondingly, the lattice fringes with spacing of 0.22 and 0.28 nm can be identified for Pt(111) and ZnO(100) planes, respectively. More importantly, it was found that the sizes of Pt clusters are greatly dependent on the applied power of ultrasonic irradiation as shown in Figure 2c. With the increase of ultrasonic power from 160 to 400 W, the average diameter of Pt clusters decreases from 2.5 to 1.1 nm, and the size distribution also becomes narrower as shown in the insets. Such good correlation between applied power and resulted Pt diameter gives us a very facile way to achieve the fine adjustment of such metal/oxide composite nanocages, matching the requirement of performance.

The formation of the Pt/ZnO porous nanocages is the result of the $H_2PtCl_6-C_4H_6O_6$ two-step etching process as shown in Figure 3a. It was believeed that the first H_2PtCl_6 etching induces the core hollowing and Pt incorporating, and the latter $C_4H_6O_6$ etching induces the nanoshell opening. Generally, well-crystallized ZnO is stable in weak acidic solution; however, considering ZnO's amphoteric feature and the starting ZnO nanoshells' ordered/disordered (fine crystalline grains surrounded by the amorphous matrix) microstructure, the etching reaction would be significant. Such a total formation mechanism has been verified by the results shown in Figure 4. First, the one-step H_2PtCl_6 etching surely results in the Pt/ZnO hollow nanoparticles, but all of them have ac losed shell as shown in Figure 4a. However, the two-step $H_2PtCl_6-C_4H_6O_6$ etching with insufficient $C_4H_6O_6$ forms the Pt/ZnO porous nanocages as shown in Figure 4b. It can be found that the insufficient $C_4H_6O_6$ content leads the shell opening extent here to not be as intensive as that in the sufficiently etched sample in Figure 1.

$$2Zn + Pt^{4+} \rightarrow 2Zn^{2+} + Pt^0 \quad (1)$$

For the first step of H_2PtCl_6 etching, the main chemical reaction will be the rapid replacement reaction between metal Zn cores and Pt ions, as shown in formula 1, due to their large difference in chemical potentials. This is the main inducement for the hollowing of core parts in the primal nanoparticles. As the indispensable condition for this replacement reaction, the ionic diffusion through the shells is needed and considered to be accompanied with the particle deposition in the shells.

On one hand, considering the small ionic diameter of Pt and the boundary-rich ZnO shell,[19] it should be easy for Pt^{4+} ions to diffuse through the shells along the grain boundaries. On the other hand, the deoxidized Pt^0 will be in situ deposited. In the system composed of surrounding Pt^{4+} ion solution, grain boundary channels in the ZnO shell, and an inner metal Zn core,

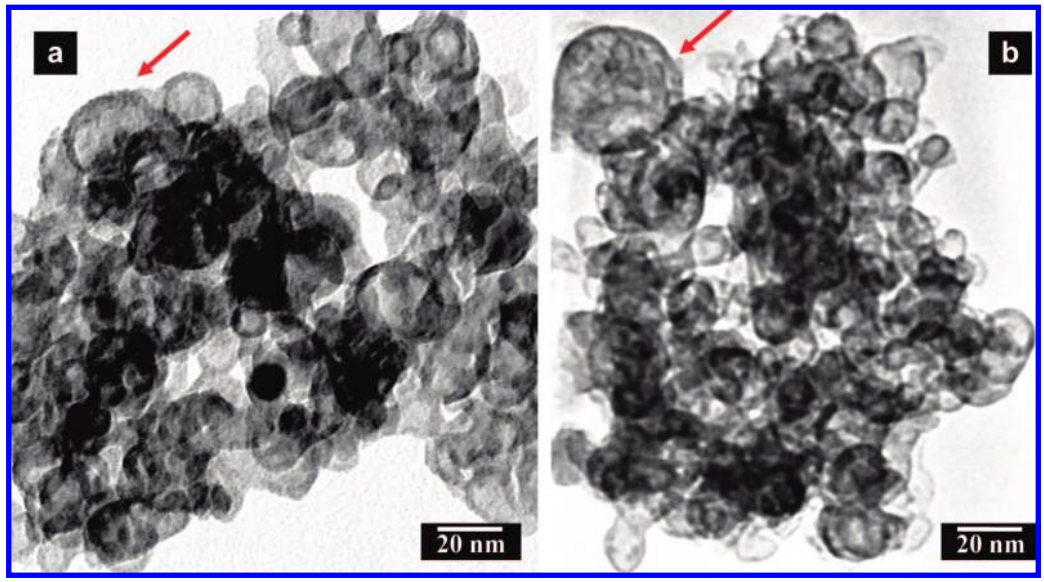

Figure 4. TEM images of closed hollow nanoparticles (a) by H_2PtCl_6 one-step etching and porous nanocages (b) by $C_4H_6O_6$-insufficient two-step etching. The added arrows point out the typical closed nanoshells and porous nanocages.

there exists large concentration gradients for both Pt and Zn. Considering the ultrafine size of channels along the grain boundary (the shell thickness is as small as 3 nm), such material density gradients will greatly affect the diffusion of Pt and Zn and induce the two-way diffusion of Pt (inward) and Zn (outward), which leads the deoxidized Pt^0 to be deposited in the channels but not in the core parts, forming the embedded Pt nanoparticles, as shown in Figure 3b. At least, such two-way diffusion would take place in the channel segment near the inner wall. This process is similar to that in the nanoscale Kirkendall effect, typically for example, $ZnAl_2O_4$ nanotubes formed by solid phase reaction and two-way diffusion of $ZnO-Al_2O_3$.[20,21] The ultrasonic irradiation also takes an important role to provide the strong driving force and dispersing function. The increased ultrasonic power would elevate the reaction rate and sites. The corresponding size reduction of Pt nanoparticles could be ascribed to the ultrasonic irradiation-induced more homogeneous occurrence of the diffusion−redox−deposition process in more diffusion channels, which reduces the involved ion number in each channel and hence the size of the precipitated Pt nanoparticles.

Finally, the $C_4H_6O_6$ etching in the second step induces the ZnO shell opening, which is the result of the weak reaction of weak acid with ZnO due to its amphoteric feature as the following formula (2). Those grain boundaries acting as diffusion channels would be preferentially enlarged by the H^+ etching as shown in Figure 3c. This has been well demonstrated by Figure 4b. It was found that the stronger acid will induce the rapid cataclasm of ZnO shells, but the weaker acid cannot induce the shell opening. The selections of type, concentration, and content of acid are important to form the porous nanocages.

$$ZnO + 2H^+ \leftrightarrow Zn^{2+} + H_2O \quad (2)$$

From the above description, two outstanding features of these metal/semiconductor composite nanocages are worthy of being noticed. On one hand, considering the small size and high density of these Pt clusters, without doubt, a great mass of metal−semiconductor (Pt−ZnO) interfaces have been constructed in the final composite nanocages. In other words, abundant Schottky barriers have been formed, which would endue these nanocages with strong separating ability for the photogenerated charges.[5−7] Moreover, the embedding state of noble metal, rather than usual surface attachment, would further improve the effective interfaces and further favor such separating ability. On the other hand, the hollow and porous structure would greatly increase the specific surface area and active sites for reaction. Also, the adsorption ability will be improved. Thus, these Pt/ZnO porous nanocages could have remarkable performance in charge-separating favored fields, such as photocatalysis.

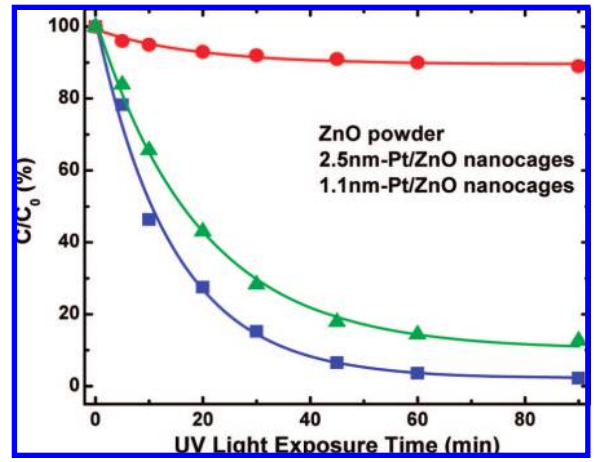

Figure 5. MO photodegradation rate of Pt/ZnO porous nanocages with different Pt cluster diameter, compared with common ZnO powder.

The results of photocatalytic degradation of methyl orange using Pt/ZnO nanocages are presented in Figure 5, compared with commercial ZnO powder (with particle diameter from 500 to 2000 nm). Obviously, the Pt/ZnO nanocages have much better photocatalytic activity than the common ZnO powder. Furthermore, the photocatalytic efficiency of the nanocages slightly increases with the reduction of Pt cluster size. Especially, for the 1.1 nm Pt/ZnO nanoshells, the polymer was quickly degraded about 90% in 40 min in our experimental conditions. As mentioned above, such improved photocatalytic activity can be attributed to the more effective electron−hole separation and larger specific surface area due to the special structure of these Pt/ZnO porous nanocages. Such great improvement of photocatalysis performance implies their great potential application in purification of pollution in water or air.

Conclusion

In conclusion, the reported method based on ultrasonic irradiation-assisted two-step etching of core/shell nanoparticles is facile and effective to fabricate Pt/ZnO porous nanocages. The first H_2PtCl_6 etching induces the core hollowing and Pt incorporating through the diffusion−redox−deposition process, and the latter $C_4H_6O_6$ etching induces the nanoshell opening due to ZnO's amphoteric feature. These Pt/ZnO porous nanocages have very small size parameters (with diameter of 20 nm and shell thickness of 3 nm). The Pt cluster size can be further reduced to as small as about 1 nm by the increased ultrasonic power. These Pt/ZnO porous nanocages show enhanced photocatalytic activity, which is due to the more effective electron−hole separation and larger specific surface area in the Pt/ZnO nanocages. Remarkably, in view of the simpleness of the etching process, this etching route would be of considerable universality for fabrication of a series of noble metal/oxide porous nanocages as photocatalysts, such as the (Au, Ag, Pt, Pd)/(ZnO, TiO_2) system.

Acknowledgment. This work is financially supported by NSFC (Grant No. 10604055 and 50671100), the National Basic Research Program of China (Grant No 2007CB936604), and the Knowledge Innovation Program of the Chinese Academy of Sciences (Grant No. KJCX2-SW-W31).

References and Notes

(1) Carraway, E. R.; Hoffman, A. J.; Hoffmann, M. R. *Environ. Sci. Technol.* **1994**, *28*, 778.

(2) Jang, E. S.; Won, J. H.; Hwang, S. J.; Choy, J. H. *Adv. Mater.* **2006**, *18*, 3309.

(3) Kuo, T. J.; Lin, C. N.; Kuo, C. L.; Huang, M. H. *Chem. Mater.* **2007**, *19*, 5143.

(4) Sakthivel, S.; Neppolian, B.; Shankar, M. V.; Arabindoo, B.; Palanichamy, M.; Murugesan, V. *Sol. Energy Mater. Sol. Cells* **2003**, *77*, 65.

(5) Linsebigler, A. L.; Lu, G.; Yates, J. T. *Chem. Rev.* **1995**, *95*, 735.

(6) Maeda, K.; Takata, T.; Hara, M.; Saito, N.; Inoue, Y.; Kobayashi, H.; Domen, K. *J. Am. Chem. Soc.* **2005**, *127*, 8286.

(7) Chen, S.; Ingram, R. S.; Hostetler, M. J.; Pietron, J. J.; Murray, R. W.; Schaaff, T. G. J.; Khoury, T.; Alvarez, M. M.; Whetten, R. L. *Science* **1998**, *280*, 2098.

(8) Wood, A.; Giersig, M.; Mulvaney, P. *J. Phys. Chem. B* **2001**, *105*, 8810.

(9) Subramanian, V.; Wolf, E. E.; Kamat, P. V. *J. Phys. Chem. B* **2003**, *107*, 7479.

(10) Wu, J. J.; Tseng, C. H. *Appl. Catal. B: Environ.* **2003**, *42*, 187.

(11) Hirakawa, T.; Kamat, P. V. *J. Am. Chem. Soc.* **2005**, *127*, 3928.

(12) Height, M. J.; Pratsinis, S. E.; Mekasuwandumrong, O.; Praserthdam, P. *Appl. Catal. B: Environ.* **2003**, *42*, 187.

(13) Li, H.; Bian, Z.; Zhu, J.; Huo, Y.; Li, H.; Lu, Y. *J. Am. Chem. Soc.* **2007**, *129*, 4538.

(14) Ye, C. H.; Bando, Y.; Shen, G. Z.; Golberg, D. *J. Phys. Chem. B* **2006**, *110*, 15146.

(15) Wan, Q.; Wang, T. H. *Appl. Phys. Lett.* **2005**, *87*, 083105.

(16) Cao, X. L.; Zeng, H. B.; Wang, M.; Xu, X. J.; Fang, M.; Ji, S. L.; Zhang, L. D. *J. Phys. Chem. C* **2008**, *112*, 5267.

(17) Wang, W. W.; Zhu, Y. J.; Yang, L. X. *Adv. Funct. Mater.* **2007**, *17*, 59.

(18) Zeng, H. B.; Cai, W. P.; Liu, P. S.; Xu, X. X.; Zhou, H. J.; Klingshirn, C.; Kalt, H. *ACS Nano* **2008**, *2*, 1661.

(19) Zeng, H. B.; Cai, W. P.; Li, Y.; Hu, J. L.; Liu, P. S. *J. Phys. Chem. B* **2005**, *109*, 18260.

(20) Fan, H. J.; Knez, M.; Scholz, R.; Nielsch, K.; Pippel, E.; Hesse, D.; Zacharias, M.; Gosele, U. *Nat. Mater.* **2006**, *5*, 627.

(21) Fan, H. J.; Knez, M.; Scholz, R.; Hesse, D.; Nielsch, K.; Zacharias, M.; Gosele, U. *Nano Lett.* **2007**, *7*, 993–997.

JP807309S